

ANALYSIS OF THE ENERGETIC/ENVIRONMENTAL PERFORMANCES OF GAS TURBINE PLANT – EFFECT OF THERMAL BARRIER COATINGS AND MASS OF COOLING AIR

by

**Ion V. ION, Anibal PORTINHA, Jorge MARTINS,
Vasco TEIXEIRA, and Joaquim CARNEIRO**

Original scientific paper

UDC: 662.951.2:66.011

BIBLID: 0354-9836, 13 (2009), 1, 147-164

DOI: 10.2298/TSCI0901147I

Zirconia stabilized with 8 wt.% Y_2O_3 is the most common material to be applied in thermal barrier coatings owing to its excellent properties: low thermal conductivity, high toughness and thermal expansion coefficient as ceramic material. Calculation has been made to evaluate the gains of thermal barrier coatings applied on gas turbine blades. The study considers a top ceramic coating Zirconia stabilized with 8 wt.% Y_2O_3 on a NiCoCrAlY bond coat and Inconel 738LC as substrate. For different thickness and different cooling air flow rates, a thermodynamic analysis has been performed and pollutants emissions (CO , NO_x) have been estimated to analyse the effect of rising the gas inlet temperature. The effect of thickness and thermal conductivity of top coating and the mass flow rate of cooling air have been analysed. The model for heat transfer analysis gives the temperature reduction through the wall blade for the considered conditions and the results presented in this contribution are restricted to a two considered limits: (1) maximum allowable temperature for top layer (1200 °C) and (2) for blade material (1000 °C). The model can be used to analyze other materials that support higher temperatures helping in the development of new materials for thermal barrier coatings.

Key words: *thermal barrier coatings, zirconia, gas turbines, heat transfer, thermal and exergetic efficiency, irreversibility, pollutant emissions*

Introduction

In order to increase the thermal efficiency of a gas-turbine cycle (two ways are possible assuming the basic efficiency equation $\eta = 1 - T_{\min.}/T_{\max.}$ – Carnot efficiency): decreasing $T_{\min.}$ and increasing $T_{\max.}$. The first is limited by the ambient temperature T_0 and by the size of the air preheater surface. The increase of $T_{\max.}$ creates strength problem on the blades and vanes material. It is possible to avoid these problems by keeping the blades and vanes material temperature below $T_{\max.}$, using coated blades and vanes or/and cooling these elements by air from the air compressor [1]. When air cooling technique is used, a higher combustion temperature is required to compensate the cooling effect of the cooling air.

Zirconia (ZrO_2) stabilized with 8 wt.% Y_2O_3 is the most common material to be applied in thermal barrier coatings (TBC) owing to its excellent properties: low thermal conductivity; high toughness and thermal expansion coefficient similar to the substrate and intermediate metallic coatings, good wear and erosion resistance and a good resistance to thermal shocks.

TBC's improve performance at high temperatures [2-4], allowing higher inlet temperatures for the same cooling rates or even reducing and simplifying the cooling systems [3, 5]. Also, with the increase of hot gas temperature some benefits concerning reduction of emissions like the unburned hydrocarbons and CO are expected. However, the nitrogen oxide NO_x emissions would tend to increase [6]. Nowadays the requests for emissions reduction (nitrogen oxides, carbon oxide, and unburned hydrocarbons) are very important. The abatement of NO_x emissions, can be achieved by the control of flame temperature (staged combustion, injection of water and steam into the flame), by improving the combustors design or by catalytic reactions.

Super alloy developments (with directional and single crystal solidification) allow its operation above 1000°C (1273 K) under higher stresses. However to achieve higher thermal efficiencies and power the highly thermal loaded parts of gas turbines are usually protected with a MCrAlY (M-Ni, Co) bond coat coating which provides oxidation protection and better thermo-mechanical compatibility with a ceramic TBC which most of the time is a partially stabilised zirconia (ZrO_2 -8 wt.% Y_2O_3) with about 300 μm thickness. As is well known, the ZrO_2 -8 wt.% Y_2O_3 coatings are not able to operate continuously above 1200°C (1473 K) because of the sintering effects. TBC's sintering reduces the porosity, allowing the increase in elastic modulus and residual stresses that reduces the fracture toughness. These effects associated with the thermally growth oxide leads to an early failure of the coating [7-12]. Another effect of working at higher temperatures is related with the phase stability. At high temperatures the non transformable tetragonal zirconia (t') tends to transform to the tetragonal and cubic phase ($t+c$) and under the cooling it transforms to monoclinic that is accompanied by a 3 to 5% volume expansion of unitary cell, and this volume expansion can cause high residual stresses and micro cracks leading to delaminating and spallation of coatings [13].

Nowadays with the purposes of further increase the efficiency of gas turbines plants new high temperature stable materials are required. These materials should improve the thermal gradient in the hot sections for the same or simplified cooling systems, for high gas inlet temperatures and should have the good combination of properties as zirconia. For this purpose, materials with lower thermal conductivities have been developed in the recent years, consisting on the additions of some rare earth materials to the base zirconia coatings, changing the architecture of the coatings (layered structures and graded materials in composition and in porosity), by the nanocomposite coatings, and new materials like lanthanide group materials [14-19].

In thermal barrier coatings applications, the heat transfer by conduction has the most important contribution. That is why the thermal conductivity of thermal barrier coatings is a very important parameter to calculate the heat flow and the temperature gradient of the coated parts [20].

In order to estimate the effect of thermal conductivity, the plasma sprayed zirconia thermal barrier coatings with a thermal conductivity values, k_1 in the range 0.5-1.2 W/mK were considered. In the case of gas turbines, the thermal conductivity values for TBC's are 0.8 to 1 W/mK which is a function of the porosity level [21].

To find out the effect of thermal barrier coatings application on turbine blades, calculation has been made for the gain in thermal efficiency and net power of the turbine plants. A detailed description of the results function of thermal conductivity, thickness of the top coat, and the mass flow rate of cooling air is presented. The application of thermal barrier coatings allows a reduction of the temperature on metal parts, increasing their life time and improving the gas turbines performances.

Thermodynamic analysis

With the purpose to perform energy and exergy analyses of a gas turbine plant it was considered the gas turbine plant with regeneration shown in fig. 1, which works under the

Joule-Brayton cycle. The parameters of the characteristic points are given in the enclosed table. The working processes of the Joule-Brayton cycle are: isentropic compression of the air at atmospheric temperature and pressure (1-2); isobaric air preheating (2-3); isobaric combustion (3-4); isentropic expansion (4-5), and isobaric cooling of flue gas (5-6). The process (6-1) is fictive, as the exhaust gases exit at point 6 and fresh air enters at point 1. In this analysis the temperature dependent working fluids properties ($c_{p,a}$, $c_{p,g}$) were considered to describe more realistically the plant operation.

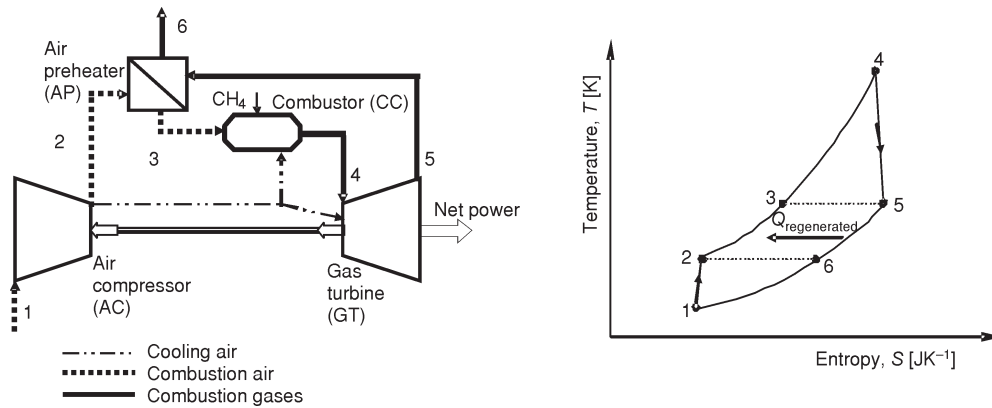


Figure 1. Gas turbine plant working under the Joule-Brayton cycle

Properties of the steams		
Flow	T [K]	p [bar]
1	298.15	1.013
2	659.55	12
3	943.3	11.4
4	1637	10.83
5	1014.2	1.099
6	794.5	1.066

Energy analysis

For the considered plant, the gas turbine power \dot{W}_{GT} , air compressor power \dot{W}_{AC} , net power \dot{W}_{net} and thermal efficiency (first law efficiency) h_1 are given by the following eqs. [22-24]:

Air compressor power

$$\dot{W}_{AC} = \dot{m}_a (1 - \beta) [c_{p,a}(T_2)T_2 - c_{p,a}(T_1)T_1] \tag{1}$$

where

$$T_2 = T_1 \left[1 + \frac{1}{\eta_{AC}} \left(\frac{p_2}{p_1} \right)^{\frac{\gamma_a - 1}{\gamma_a}} - 1 \right] \tag{2}$$

γ_a – air specific heat ratio, $\gamma_a = c_{p,a}/(c_{p,a} - R_a)$;
 $\eta_{AC} = 0.8468$, air compressor isentropic efficiency [22].

The specific heat as a function of temperature (temperature range: 273-1800 K) is calculated for the different gases as is shown in tab. 1 [23].

Table 1. Ideal-gas specific heats of various gases

$c_p(T) = A_0 + B_0T + C_0T^2 + D_0T^3$					
Substance	Formula	A_0	B_0	C_0	D_0
Air	–	0.97034	$0.6789 \cdot 10^{-4}$	$1.657 \cdot 10^{-7}$	$-6.786 \cdot 10^{-11}$
Nitrogen	N ₂	1.0316	$-0.5608 \cdot 10^{-4}$	$2.884 \cdot 10^{-7}$	$-1.0256 \cdot 10^{-10}$
Oxygen	O ₂	0.7962	$4.75 \cdot 10^{-4}$	$-2.235 \cdot 10^{-7}$	$4.1 \cdot 10^{-11}$
Water vapour	H ₂ O	1.789	$0.106 \cdot 10^{-4}$	$5.856 \cdot 10^{-7}$	$1.995 \cdot 10^{-10}$
Carbon dioxide	CO ₂	0.505	$1.359 \cdot 10^{-3}$	$-7.955 \cdot 10^{-7}$	$-1.697 \cdot 10^{-10}$

Combustor mass balance

$$\dot{m}_g = \dot{m}_a + \dot{m}_f \quad (3)$$

Combustor energy balance

$$\dot{m}_a c_{pa}(T_3)T_3 + \eta_{CC} \dot{m}_f LHV = \dot{m}_g c_{pg}(T_4)T_4 \quad (4)$$

The flue gas specific heat is given by the equation:

$$c_{pg}(T) = \frac{1}{m_g} [c_{pCO_2}(T)m_{CO_2} + c_{pO_2}(T)m_{O_2} + c_{pH_2O}(T)m_{H_2O} + c_{pN_2}(T)m_{N_2}] \quad (5)$$

Chemical equation for methane combustion with excess air (the dissociation process is not considered):



Air preheater energy balance:

$$\dot{m}_a [c_{pa}(T_3)T_3 - c_{pa}(T_2)T_2] = \dot{m}_{g1} [c_{pg}(T_5)T_5 - c_{pg}(T_6)T_6] \quad (7)$$

where: $\dot{m}_{g1} = \dot{m}_g + \beta \dot{m}_a$, $p_3 = p_2(1 - p_{aAPH})$, $p_{aAPH} = 0.05$ (pressure loss on the air path) [22]; $p_6 = p_5(1 - p_{gAPH})$, $p_{gAPH} = 0.03$ (pressure loss on the flue gas path) [22].

Gas turbine power comes as:

$$\dot{W}_{GT} = \dot{m}_g [c_{pg}(T_4)T_4 - c_{pg}(T_5)T_5] \quad (8)$$

(the cooling air does not expand in turbine) where:

$$T_5 = T_4 \left[1 - \eta_{GT} \left(1 - \frac{p_4}{p_5} \right)^{\frac{1}{\gamma_g}} \right] \quad (9)$$

Considering the previous calculations we are able to determine the net power and first law efficiency of our system.

Net power:

$$\dot{W}_{net} = \dot{W}_{GT} - \dot{W}_{AC} \quad (10)$$

First-law efficiency or thermal efficiency (the ratio of net work output and total heat input) of the gas turbine plant:

$$\eta_1 = \frac{\dot{W}_{net out}}{\dot{Q}_{in}} = \frac{\dot{W}_{net}}{\dot{m}_f LHV} = \frac{\dot{W}_{GT} - \dot{W}_{AC}}{\dot{m}_f LHV} \quad (11)$$

Exergy analysis

Exergy is a thermodynamic concept that measures the maximum amount of useful work that can be extracted when a system is brought reversibly into equilibrium (thermal, mechanical, and chemical) with the standard environment ($T_0 = 298.15 \text{ K}$, $p_0 = 1.013 \text{ bar}$) conditions.

The exergy analysis [25] given by the description bellow, was implemented in order to estimate the second-law efficiency of the gas turbine plant.

Exergy balance for air compressor

$$\dot{m}_1 e_{a1} - \dot{W}_{AC} = \dot{m}_2 e_{a2} - \dot{I}_{AC} \tag{12}$$

where the specific exergy of air streams is:

$$e_{ai} = c_{pa}(T_i)T_i - c_{pa}(T_0)T_0 - c_{pa}(T_a^{av})T_0 \ln \frac{T_i}{T_0} - R_a T_0 \ln \frac{p_i}{p_0} \tag{13}$$

$$T_a^{av} = \frac{T_i + T_0}{2}$$

Exergy balance for combustion chamber

$$\dot{m}_3 e_{a3} - \dot{m}_f e_f - \dot{m}_4 e_{g4} = \dot{I}_{CC} \tag{14}$$

$$e_{gj} = c_{pg}(T_j)T_j - c_{pg}(T_0)T_0 - c_{pg}(T_g^{av})T_0 \ln \frac{T_j}{T_0} - R_g T_0 \ln \frac{p_j}{p_0} \tag{15}$$

$$\frac{1}{m_g} \sum_k n_k \varepsilon_k^0 = 8314 T_0 \sum_k n_k \ln x_k$$

where e_f is the specific exergy of the fuel, $e_f = 51\,850 \text{ kJ/kg}$ [22]; n_k and x_k are the mol number and molar fraction of the k^{th} element, respectively (see tab. 2); $AFR = m_a/m_f$ – air-fuel ratio.

Table 2. Equations for calculating mass, mole number and mole fraction of the combustion gas constituents

Mass	Mole number	Mole fraction
$m_{CO_2} = 2.75 m_f$	$n_{CO_2} = \frac{m_{CO_2}}{M_{CO_2}}$	$x_{CO_2} = \frac{n_{CO_2}}{n_g}$
$m_{O_2} = m_f(0.21AFR - 4)$	$n_{O_2} = \frac{m_{O_2}}{M_{O_2}}$	$x_{O_2} = \frac{n_{O_2}}{n_g}$
$m_{N_2} = 0.79 m_f AFR$	$n_{N_2} = \frac{m_{N_2}}{M_{N_2}}$	$x_{N_2} = \frac{n_{N_2}}{n_g}$
$m_{H_2O} = 2.25 m_f$	$n_{H_2O} = \frac{m_{H_2O}}{M_{H_2O}}$	$x_{H_2O} = \frac{n_{H_2O}}{n_g}$
Total mass of the combustion gas	Total mole number of the combustion gas	Total mole fraction of the combustion gas
$m_g = m_{CO_2} + m_{O_2} + m_{N_2} + m_{H_2O}$	$n_g = n_{CO_2} + n_{O_2} + n_{N_2} + n_{H_2O}$	$x_{CO_2} + x_{O_2} + x_{N_2} + x_{H_2O} = 1$

Table 3. Molar standard chemical exergy

Substance	Formula	Gas constant R [kJkg ⁻¹ K ⁻¹]	Molar mass, M [kgkmol ⁻¹]	Molar standard chemical exergy, ε^0 [kJkmol ⁻¹]
Air	–	0.2868	28.97	0
Nitrogen	N ₂	0.2968	28.013	720
Oxygen	O ₂	0.2598	31.999	3970
Water vapour	H ₂ O	0.4615	18.015	11710
Carbon dioxide	CO ₂	0.1889	44.01	20140

Exergy balance for air preheater

$$\dot{m}_2 e_{a2} \quad \dot{m}_5 e_{g5} \quad \dot{m}_3 e_{a3} \quad \dot{m}_6 e_{g6} \quad \dot{I}_{AP} \quad (16)$$

Exergy balance for gas turbine

$$\dot{m}_4 e_{g4} \quad \dot{W}_{net} \quad \dot{W}_{AC} \quad \dot{m}_5 e_{g5} \quad \dot{I}_{GT} \quad (17)$$

The exergetic efficiency (the ratio of the exergy recovered or exergy of product by the exergy supplied or exergy of fuel) of the gas turbine plant is:

$$\eta_{exe} = \frac{\dot{W}_{net}}{\dot{m}_f e_f} = \frac{\dot{W}_{GJ} + \dot{W}_{AC}}{\dot{m}_t e_f} \quad (18)$$

Summing up eqs. (12-17) we obtain the available work destroyed through thermodynamic irreversibility:

$$\underbrace{\dot{m}_f e_f + \dot{m}_6 e_{g6}}_{(\dot{W}_{net})_{rev}} \quad \dot{W}_{net} \quad \dot{W}_{lost} \quad \dot{I}; \quad I \quad AC, CC, AP, GT \quad (19)$$

Equation (18) allows us to calculate the second-law efficiency (the ratio of the useful work output and the maximum possible – reversible – work output) of the gas turbine plant [1]:

$$\eta_{II} = \frac{\dot{W}_{net}}{(\dot{W}_{net})_{rev}} = 1 - \frac{\dot{I}}{(\dot{W}_{net})_{rev}} \quad (20)$$

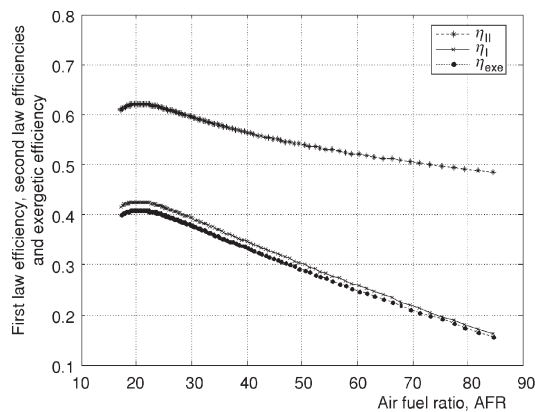


Figure 2. Efficiency changes for: cycle thermal efficiency η_I , second-law efficiency η_{II} , and exergetic efficiency η_{exe} as a function of AFR

Figure 2 shows the change of efficiency (for the 3 referred efficiencies) as a function of AFR. As predicted, there is an initial raise with a subsequent reduction of all efficiencies, as the AFR is increasing.

NO_x and CO emissions

Nowadays the environmental effect of combustion gases is an important concern and a clean combustion of fossil fuels is necessary.

In the estimation of pollutant emissions it was considered a dry low NO_x

combustor. In this combustor the emissions are reduced only by flame temperature control using a staged combustion.

The emissions are estimated using the following semi-analytical correlations [26]:

$$\text{NO}_x = \frac{15 \cdot 10^{13.75} \tau^{0.5} \exp\left(\frac{71100}{T_{pz}}\right)}{p_3^{0.05} \frac{\Delta p_{a AP}}{p_3}}, [\text{gkg}^{-1}] \quad (21)$$

$$\text{CO} = \frac{0.018 \exp\left(\frac{71100}{T_{pz}}\right)}{p_3^2 \tau \frac{\Delta p_{a AP}}{p_3}}, [\text{gkg}^{-1}] \quad (22)$$

where the adiabatic temperature in the primary zone of the combustor is:

$$T_{pz} = B \frac{1}{AFR} \frac{p_3}{p_0} \frac{T_3}{T_0} \psi^z \exp[\beta(\sigma + 1)^2] \quad (23)$$

and ψ – the H/C atomic ratio (for methane $\psi = 4$); x, y, z – the quadratic functions of $1/AFR$ [6]; B, α, β , and λ – constants [6]; τ – the residence time in the combustor ($\tau = 0.002$ s) [26].

Heat transfer analysis

Internal cooling channels for modern rotor blade are extremely complex and they necessitate numerically study for the turbulent flow and heat transfer. In order to estimate the temperature evolutions of a multilayered structure a simplified analysis was performed considering a one-dimensional heat transfer model [27]. Figure 3 represents a cross-section of the blade in the longitudinal and transversal direction as well as the heat flux through the blade and an example of the temperature evolution through the wall blade and along the blade. The considered cooling system is an open air-cooling circuit scheme. Under steady-state conditions, the rate of heat transfer through the wall must be in equilibrium with the rate of heat transfer out.

Because of the low thermal conductivity of substrate, the heat flux along the blade is neglected. The radiation heat flux from the substrate to the cooling air is also neglected, due to the small volume of the cooling air.

For convection heat transfer we have chosen the following equations.

- The flow rate of heat transfer from the combustion gases to the TBC top coat wall [28]:

$$\Phi_{C1} = 0.02 \frac{k_g}{d_{hg}^{0.2}} \frac{\dot{m}_g}{S_g \mu_g} (T_g - T_{s1}) A_g \quad (24)$$

- The flow rate of heat transfer from the substrate inner wall to the cooling air [29]:

$$\Phi_{C2} = 0.023 \frac{k_c}{d_{hc}} \frac{\dot{m}_c d_{hc}}{S_c \mu_c} \frac{\mu_c c_{pc}}{k_c} (T_{s4} - T_c) A_c \quad (25)$$

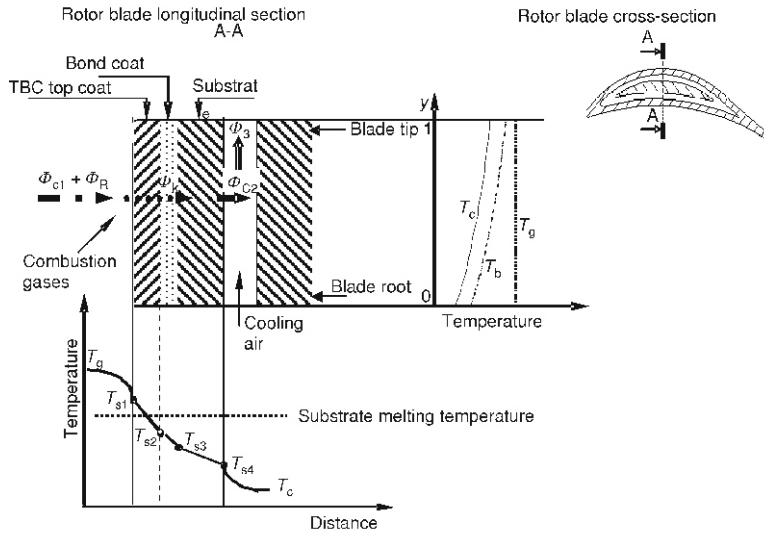


Figure 3. Heat transfer model for forced convection air cooling of rotor blade

The rate of *radiation heat transfer* from no luminous gas is given by:

$$\Phi_R = 0.5\sigma(1 - \epsilon_w)(\epsilon_g T_g^4 - \alpha_g T_{sl}^4)A_g \quad (26)$$

where

$$\epsilon_g = 1 - \exp\left(-\frac{290}{AF} l_b\right) T_g^{1.5} \quad (27)$$

$$l_b = 3.6 \text{ volume per surface area}$$

It is shown in [28] that:

$$\frac{\alpha_g}{\epsilon_g} = \frac{T_g^{1.5}}{T_{sl}} \quad (28)$$

Substituting (27) in (25) we obtain:

$$\Phi_R = 0.5\sigma\epsilon_g T_g^{1.5}(1 - \epsilon_w)(T_g^{2.5} - T_{sl}^{2.5})A_g \quad (29)$$

The rate of conduction heat transfer through the wall blade is:

$$\Phi_K = \frac{T_{s1} - T_{s2}}{\frac{\delta_1}{k_1}} + \frac{T_{s2} - T_{s3}}{\frac{\delta_2}{k_2}} + \frac{T_{s3} - T_{s4}}{\frac{\delta_3}{k_3}} + \frac{T_{s1} - T_{s4}}{\frac{\delta_1}{k_1} + \frac{\delta_2}{k_2} + \frac{\delta_3}{k_3}} \quad (30)$$

Solving the equation expressing the equilibrium between the rate of heat transfer through the wall must and the rate of heat transfer out we obtain temperature distribution in the blade wall at the blade root for a given combustion gases temperature and a given cooling air mass flow:

$$\dot{m}_c c_{pc} \frac{dT_c}{dx} = \Phi_{C2} - \Phi_K - \Phi_{C1} - \Phi_R \quad (31)$$

where dT_c/dx is temperature variation of cooling air along the blade.

From these equations we can determinate the cooling air temperature at the blade outlet:

$$T_{ct} = T_g - (T_g - T_{cr}) \exp(-M) \quad (32)$$

$$M = \frac{h_g}{\dot{m}c_{pc}(1-P)}, \quad P = \frac{h_g A_g}{h_c A_c}, \quad h_g = 0.02 \frac{k_g}{d_{hg}^{0.2}} \frac{\dot{m}_g}{S_g \mu_g}^{0.8},$$

$$h_c = 0.023 \frac{k_c}{d_{hc}} \frac{\dot{m}_c d_{hc}}{S_c \mu_c}^{0.8} \frac{\mu_c c_{pc}}{k_c}^{0.4}$$

With this new value of T_c the temperature distribution across the blade wall at the blade tip can be calculated. The values of the various parameters used for the simulations are presented in tab. 4.

Table 4. Values used in the heat transfer model simulations

Parameter	Value
Blade length, [m]	0.0845
Blade width, [m]	0.04
Blades step (distance between two blades)	0.02
TBC top coat thickness (δ_1), [m]	$300 \cdot 10^{-6} - 500 \cdot 10^{-6}$
Bond coat thickness (δ_2), [m]	$150 \cdot 10^{-6}$
Substrate thickness (δ_3), [m]	0.001
Cooling air channel thickness, [m]	0.001
Thermal conductivity of TBC top coat (k_1), [$\text{kWm}^{-1}\text{K}^{-1}$]	$0.5 \cdot 10^{-3} - 1.2 \cdot 10^{-3}$
Thermal conductivity of bond coat (k_2) at 900 K, [$\text{kWm}^{-1}\text{K}^{-1}$]	$1 \cdot 10^{-2}$
Thermal conductivity of substrate (k_3) at 800 K, [$\text{kWm}^{-1}\text{K}^{-1}$]	$15.57 \cdot 10^{-3}$
Combustion gases thermal conductivity (k_g) at 1300 K, [$\text{kWm}^{-1}\text{K}^{-1}$]	$0.157 \cdot 10^{-3}$
TBC top coat emissivity (ϵ_w) [29]	0.7
Combustion gases dynamic viscosity at 1200 K (μ_g), [$\text{kgm}^{-1}\text{s}^{-1}$]	$7.05 \cdot 10^{-5}$
Air dynamic viscosity (μ_c) at 600 K, [$\text{kgm}^{-1}\text{s}^{-1}$]	$3.03 \cdot 10^{-5}$
Gas pressure (p), [kPa]	700
Blades number in a row	69
Percentage of cooling air [%]	1-2
Gas inlet temperature [K]	1300-2000

Results and discussion

Effect of TBC's on temperature distribution through the wall blade

The calculation made for the heat transfer on the first stage blades gives the temperature on the surface of the thermal barrier coating T_{s1} and at the various interfaces with the other intermediate coatings and substrate T_{s2} , T_{s3} , and on the internal surface of substrate T_{s4} which is cooled by the cooling air that also increases its temperature towards the blade tip. Only the first stage blades are considered because they are adjacent to the combustor, where the gases have the highest temperature.

This analysis was done for gas inlet temperatures T_g in the range from 1300 to 2000 K and a constant temperature of cooling air ($T_c = 600$ K) on the blade root.

In the presented results two limits were considered:

- (1) 1200 °C (1473 K) for the maximum temperature for the partially stabilized ZrO₂-8 wt.% Y₂O₃ coatings, because above this temperature the sintering effects are more pronounced and the non-transformable tetragonal zirconia tends to transform to the tetragonal phase and under the cooling down transforms to monoclinic causing all the well known ominous effects, and
- (2) 1000 °C (1273 K) for the maximum substrate (Inconel 738 LC) temperature, in order to guarantee the thermo-mechanical strength.

The influence of the thermal conductivity k_1 , thickness δ_1 of the top zirconia coating and the percentage of the mass of air cooling rate were studied showing for each case the temperature gradient through the wall blade and the maximum gas inlet temperature allowed considering the limits previously established. Calculations were done for the thermal conductivity values in the range 0.5-1.2 W/mK. However the values for plasma sprayed coatings ranges 0.8-1 W/mK. Concerning the zirconia coating, three thicknesses δ_1 were considered: 300, 400, and 500 μ m. Typically this application uses 300 μ m and for coatings with thickness up to 500 μ m they tend to spill early due to the poor adhesion. Three values for the mass of air cooling rate were also used (1, 1.5, and 2%).

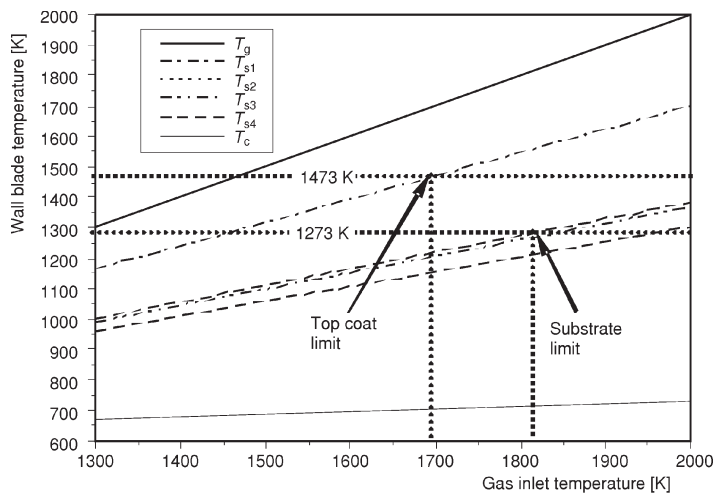


Figure 4. Temperature distribution in the wall blade (at blade tip) for different inlet temperatures

Figure 4 shows an example for the results of the model at the blade tip position that is the critical zone because the gas temperature is the same along the blades but the air cooling temperature increases from blade root to blade tip where the cooling effect is less effective. In the figure, the temperature in each position of the wall blade is plotted for different inlet temperatures.

The influence of the various parameters on the temperature distribution through the wall blade, shown in figs. 5 to 8, was determined from the previous results and for the considered limits.

In fig. 5 the temperature gradients across the wall blade section are plotted as function of the mass flow rate of blade cooling air, considering the limit temperature at the surface of the top coat equal to 1200 °C (1473 K). It was observed an increase in the temperature gradient as \dot{m}_c is increased for the three analyzed conditions.

An increase in the temperature gradient was also observed when the thickness of the top coat was enlarged, even with an increase in the thermal conductivity. For the same limit of the surface temperature on the top coat, a rise from 1652 to 1736 K is observed in gas inlet tem-

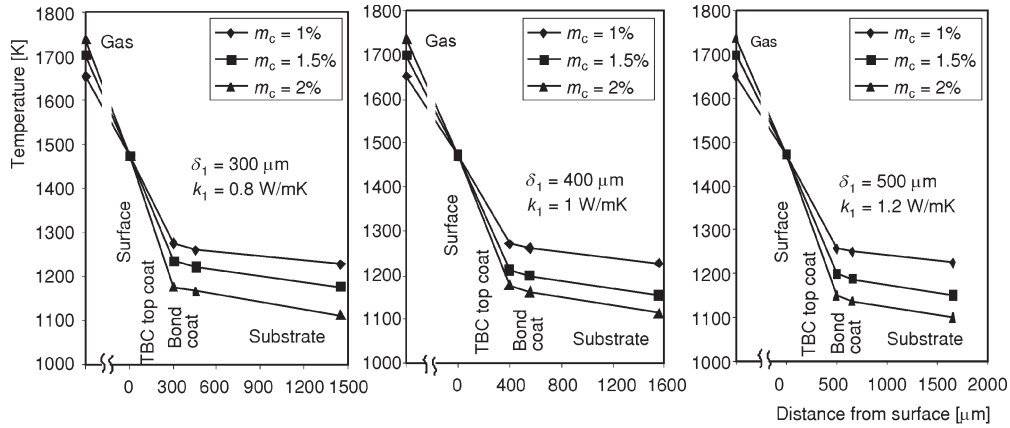


Figure 5. Temperature gradients in the wall blade cross-section considering different ZrO_2 -8 wt.% Y_2O_3 top layer thickness δ_1 and different thermal conductivity k_1 of the top layer showing the effect of the mass flow rate of cooling air \dot{m}_c

perature T_g for higher \dot{m}_c that increases with a 1% of \dot{m}_c variation in the first conditions. For other conditions the increase is similar.

Figure 6a shows the temperature reduction in the top layer at different thickness for different conditions of thermal conductivity and mass flow rate of blade cooling air \dot{m}_c . For the same conditions an increase in the temperature reduction was observed (about 78 K) with the increase of thickness through 300 to 500 μm . This increase is due the higher insulation produced by the thicker layer.

Three settings were tested in order to represent the best, medium, and worst conditions for each thickness. These are the lowest \dot{m}_c and the highest k_1 , the highest \dot{m}_c and the lowest k_1 , and intermediate values. Increasing k_1 and reducing \dot{m}_c significantly reduces the temperature gap in the top layer. Analyzing the fig. 6b the gas inlet temperature has to decrease for thicker layers, for the lower and intermediate thermal conductivity and higher mass flow rate of cooling air. However, for $k_1 = 1.2$ W/mK and $\dot{m}_c = 1\%$ the results are inverse. For the conditions where the decrease in inlet temperature was imposed, lower temperatures in the metal zone of the blade

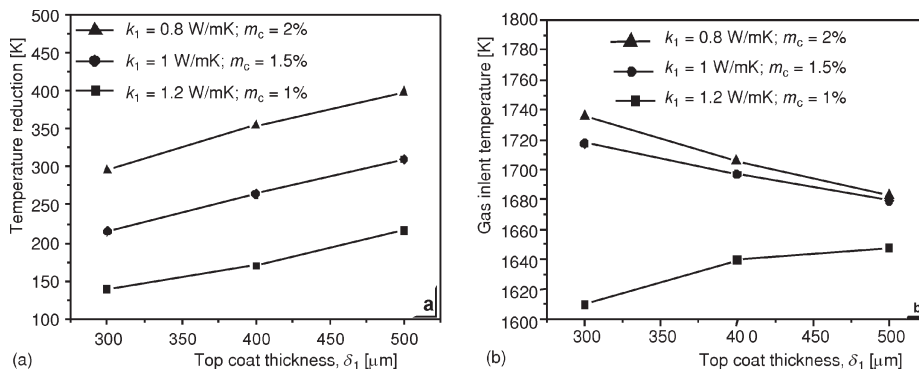


Figure 6. Temperature gradients in the top layer ZrO_2 -8 wt.% Y_2O_3 and gas inlet temperature evolution function of thickness of top layer δ_1 , for different thermal conductivity k_1 and mass flow rate of cooling air \dot{m}_c

were observed, which is good for the resistance. However this reduction on inlet temperature gives lower efficiency of the gas turbine plant.

Figure 7 shows the results of the wall blade temperature distribution for different thermal conductivity of the $ZrO_2-8 \text{ wt.}\% Y_2O_3$, for three pairs of δ_1 and \dot{m}_c , in order to show the minimum and maximum effects. The thermal conductivity is increased from $k_1 = 0.5$ to 1.2 W/mK , and this led to the reduction of the coating insulation capacity, therefore increasing the metal temperature. This effect allows a decrease in duration of the lifetime of the blade by reducing its thermal fatigue.

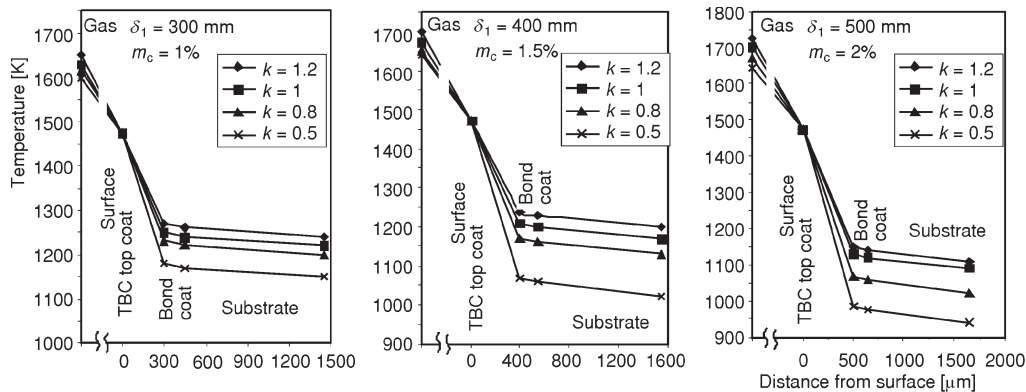


Figure 7. Temperature gradients in the wall blade cross-section for different $ZrO_2-8 \text{ wt.}\% Y_2O_3$ top layer thickness δ_1 , for different mass flow rate of cooling air \dot{m}_c showing the effect of thermal conductivity of the top layer k_1

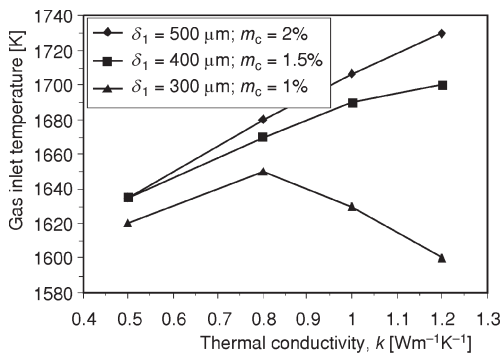


Figure 8. Inlet temperature variation with thermal conductivity of top coat for different top coat thickness and mass flow rate of cooling air

As it is shown in the fig. 8, the increase of the thermal conductivity allows the raise of the inlet temperature (gas temperature). However, for the lower thickness and lower air flow rate, the inlet temperature should be reduced because the heat flux removed by the air is not enough.

The usual thickness for plasma sprayed thermal barrier coatings in gas turbines blades is $300 \text{ }\mu\text{m}$ and the typical thermal conductivity is 0.8 W/mK . Yet, coating sintering increases the thermal conductivity, therefore reducing the insulation capabilities.

Thermodynamic results

As eq. (4) shows, we can increase the inlet temperature in the gas turbine T_4 either by increasing the mass fuel flow rate \dot{m}_f or by reducing the mass air flow rate \dot{m}_a . In this analysis it was chosen the increasing of gas turbine inlet temperature by variation of mass rate of fuel flow from 1.627 to 8 kg/s . The maximum possible inlet temperature occurs for stoichiometric combustion and depends on the LHV of the fuel.

The net output power of gas turbine plant increases with the increasing of gas turbine inlet temperature (see fig. 9), this augmentation being almost linear and for each increase of 100 K it increases nearly 120 MW. The first-law efficiency η_I , the second-law efficiency η_{II} , and the exergetic efficiency η_{exe} also increase with the inlet temperature. Compared with the first-law efficiency (the exergetic efficiency has a similar variation with gas turbine inlet temperature), the second law efficiency increases more slowly with the rise of the inlet temperature and it shows higher values.

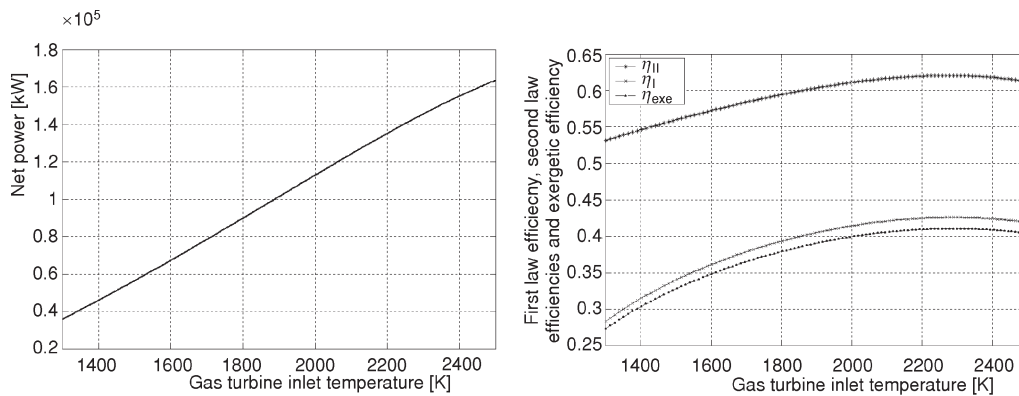


Figure 9. Variation of the net power \dot{W}_{net} , cycle thermal efficiency η_I , second-law efficiency η_{II} , and exergetic efficiency η_{exe} with the gas turbine inlet temperature

We can see in fig. 10 that for an increase of gas turbine inlet temperature of 173 K (from 1600 to 1773 K), the thermal efficiency decreases about 3%. This figure also shows that η_I decreases from 38.6% to 34.6% at 1600 K and from 41.5% to 38.2% at 1773 K, as the fraction of cooling air flow rate changes from 7% to 15%. The variation of \dot{W}_{net} with the mass of cooling air can be seen in fig. 10 and this power decreases as the fraction of cooling air flow rate raises.

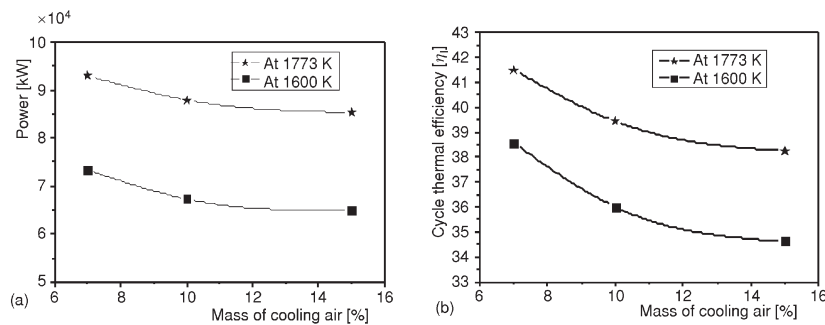


Figure 10. Variation of the net power \dot{W}_{net} and cycle thermal efficiency η_I , at the minimum (1600 K) and at the maximum (1773 K) inlet temperature, as a function of the fraction of cooling air β

It is well known that the second law analysis (exergy analysis) offers a better understanding of what is happening during a process and indicates the causes of the inefficiencies with this purpose. A second law analysis was performed for each plant component. Figure 11 shows the production of irreversibility (destruction of exergy) for each plant component and how the irreversibility rates vary with inlet temperature. The productions of irreversibility due

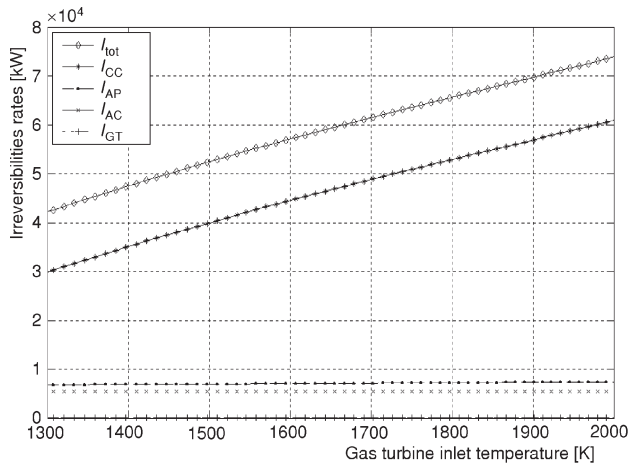


Figure 11. Total irreversibility and irreversibility of each component

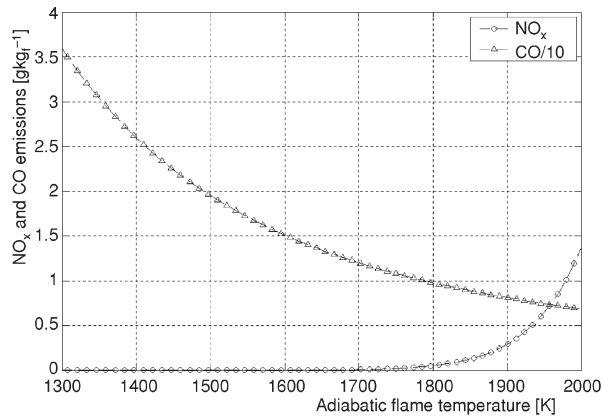


Figure 12. NO_x and CO emissions function of the adiabatic temperature in the primary zone of the combustor

The results presented in tab. 5 show that, for the same thermal conductivity and flow rate of blade cooling air, the allowed inlet temperature decreases with the increase in top layer thickness, which implies a decrease in the net power and efficiency. However the increase in the thickness of the top layer promotes better insulation, shown by the increase in the temperature difference between the surface top layer and blade material. This effect is favourable to the thermo-mechanical behaviour of the blades.

Increasing the mass flow rate of blade cooling air promotes an increase in the efficiency and in the net power because it allows higher inlet temperatures by promoting the intensification of heat removal. This raise in inlet temperature is accompanied by an increase in the insulating effect allowing, lower temperatures in the metal parts even for higher gas inlet temperatures.

The higher thermal conductivity of the thermal barrier coatings promotes an increase of the net power and the efficiencies by allowing higher inlet temperatures.

to heat transfer \dot{I}_{AP} , air compression \dot{I}_{AC} , and combustion gas expansion \dot{I}_{GT} are negligible compared to the combustion process \dot{I}_{CC} and the irreversibility creation rate in the combustor increases with the increase of inlet temperature.

The NO_x and CO emissions, function of the adiabatic flame temperature in the primary zone of the combustor, are plotted in fig. 12. This primary zone is close to the gas turbine inlet temperature. As expected the NO_x emissions increase with the combustion temperature. It is known that, as combustion temperature increases the NO_x emissions increase. The NO_x increases exponentially with the temperature above about 1750 K. Our results prove this effect, as can be seen in the NO_x curve on fig. 12.

Table 5 shows gas inlet temperature T_g , thermodynamic efficiencies (η_I , η_{II} , and η_{exe}) and net power \dot{W}_{net} as a function of mass of blade cooling air, TBC thickness and thermal conductivity for the fraction of cooling air $\beta = 10\%$. These results were obtained considering the maximum temperature allowed for the ZrO₂-8 wt.% Y₂O₃ top coating (1200 °C) and for the blade base material (Inconel 738 LC) (1000 °C).

Table 5. The correlations between mass flow rate of blade cooling air and properties of coatings in thermodynamic performances

Thickness δ_1 [mm]		300			400			500			
Mass of cooling air \dot{m}_c [%]		1	1.5	2	1	1.5	2	1	1.5	2	
Thermal conductivity, k_1 [$\text{Wm}^{-1}\text{K}^{-1}$]	0.5	T_g [K]	1625	1653	1690		1636				1635
		η_{exe} [%]	35.17	35.8	36.53		35.42				35.4
		η_I [%]	36.56	37.17	37.82		36.79				36.77
		η_{II} [%]	59.79	60.45	60.82		60.01				59.97
		\dot{W}_{net} [MW]	70.6	74.0	77.7		71.5				71.2
	0.8	T_g [K]	1652	1698	1736		1674	1706			1683
		η_{exe} [%]	35.78	36.64	37.25		36.14	36.81			36.33
		η_I [%]	37.11	37.9	38.62		37.48	38.2			37.64
		η_{II} [%]	60.43	61.01	61.61		60.68	61.13			60.79
		\dot{W}_{net} [MW]	73.5	78.8	83.4		75.9	80.0			76.0
	1.0	T_g [K]	1632	1717	1760	1650	1697	1730		1679	1707
		η_{exe} [%]	35.3	37.00	37.70	35.72	36.62	37.18		36.22	36.83
		η_I [%]	36.68	38.87	39.14	37.08	37.89	38.54		37.61	38.22
		η_{II} [%]	59.88	61.32	61.91	60.34	60.94	61.52		60.73	61.15
		\dot{W}_{net} [MW]	71.2	81.1	86.5	73.3	78.8	82.7		76.7	80.0
	1.2	T_g [K]	1600	1724	1773	1639	1705		1648	1690	1730
		η_{exe} [%]	34.61	37.11	38.00	35.44	36.79		35.67	36.53	37.18
		η_I [%]	36.00	38.43	39.43	36.82	38.17		36.97	37.82	38.54
		η_{II} [%]	59.44	61.43	62.13	60.13	61.12		60.28	60.82	61.52
		\dot{W}_{net} [MW]	67.3	82.1	87.9	72.0	79.8		73.0	77.9	82.7

However this gain is limited and in particular for the air mass flow rate of 1%, the inlet temperature can be increased only when k_1 is below 0.8 W/mK. Figure 13 also shows that the increase of thermal conductivity has an important effect in terms of the insulating effect. For example, for the 300 μm thickness, the increase in k_1 from 0.5 to 1.2 W/mK induces a decline in temperature reduction of about 150 K and the gain in inlet temperature is only about 75 K for $\dot{m}_c = 1.5$ and 2%.

For the studied conditions (fraction of cooling air flow rate $\beta = 10\%$) the possible range for the inlet temperature lies be-

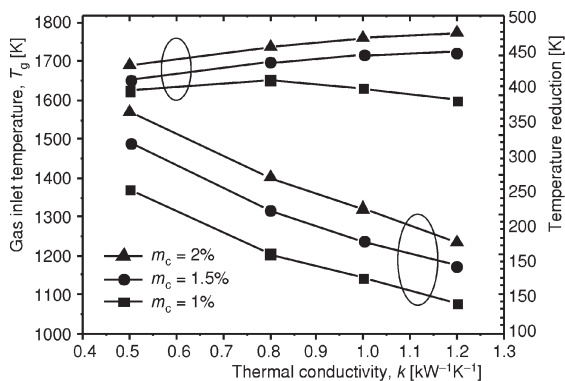


Figure 13. The correlation between the thermal conductivity of thermal barrier coatings on the reduction of blade temperature for top coating thickness of 300 μm

tween 1600 and 1773 K. Within this range it is possible to increase the net power by 20.63 MW and the thermal efficiency by 3.4%. However, a carefully analysis is necessary in order to select the combination of the thermal barrier coatings properties (k_1 and δ_1) because the lower k_1 leads to higher thermal insulation but allows lower inlet temperatures. The increase of coatings thickness also has the same effect. Please note that the reduction of k_1 and the increase of δ_1 for the same blade cooling rate lead to an important temperature reduction for the metallic parts. This metallic temperature reduction may be more important than the decrease in thermodynamic performances. Reducing k_1 from 1.2 to 0.5 W/mK promotes a decrease of about 1.4% in thermal efficiency and the increase of δ from 300 μm to 500 μm promotes a decrease of about 1%.

On the other hand, for the same maximum temperature allowed by the top coat, it is possible to increase the temperature reduction for the metallic part by near 150 K for the thickness of 300 μm and about 170 K for the thickness of 500 μm . For the same k_1 and blade cooling rate \dot{m}_c the increase in thickness of top coat from 300 to 500 μm produces an increase in temperature reduction of about 100 K.

Conclusions

In this study calculations have been made for the parametric study of various conditions and properties, including thermal conductivity of top coating, its thickness and the blade mass flow rate of cooling air.

For the thermodynamic analysis, the model is an important step forward among other studies, as it considers the temperature dependent working fluids properties ($c_{p,a}$, $c_{p,g}$) in order to describe more realistically the plant operation. Also, it considers a different mass flow rate though the compressor (just air) and the gas turbine (combustion gases), the difference being equal to the mass flow rate of the fuel.

This analysis shows that the decrease in thermal conductivity from 1.2 to 0.5 W/mK augments significantly the temperature reduction between top coat surface and metallic bond coat and leads to lower thermodynamic performances. However the gain in the temperature reduction is more important than the loss in the performance (about 1.4% in thermal efficiency). A similar effect appears with the change of thickness. Increasing the mass flow rate of blade cooling air increases the temperature reduction and the thermodynamic performance.

As expected, the increase of inlet temperature leads to the NO_x emissions increase (mainly above 1750 K) while the CO emissions decrease.

For the development of other materials that are stable at higher temperatures and for the same thermal conductivities it is possible to estimate the limiting inlet temperatures and estimate its effect on the efficiency and performance of gas turbines.

Acknowledgments

This work was financially supported by F. C. T. – Portuguese Foundation for Science and Technology under the project POCTI/EME/39316/2001: “PVD/COAT-Composite and multilayered protective coatings for efficient energy systems”.

Ion V. Ion thanks GRICES Portugal (Gabinete de Relações Internacionais da Ciência e do Ensino Superior) for the granted NATO Science Fellowship.

A. Portinha is gratefully for the research grant supported by F. C. T. – Portuguese Foundation for Science and Technology.

Nomenclature

A	– heat transfer area, [m ²]
AFR	– air-fuel ratio, [–]
c_p	– specific heat, [kJkg ⁻¹ K ⁻¹]
d	– diameter, [m]
e	– specific exergy, [kJkg ⁻¹]
I	– irreversibility rate, [kW]
k	– thermal conductivity, [kWm ⁻¹ K ⁻¹]
LHV	– lower heating value of natural gas taken as methane (50000 kJkg ⁻¹)
M	– molar mass, [kgkmol ⁻¹]
m	– mass, [kg]
\dot{m}	– mass flow rate, [kgs ⁻¹]
n	– mole number, [–]
p	– pressure, [kPa]
R	– gas constant, [kJkg ⁻¹ K ⁻¹]
S	– cross-sectional flow area, [m ²]
T	– temperature, [K]
x	– mole fraction, [–]

Greek letters

α	– absorptivity, [–]
β	– air fraction used for the cooling of combustion chamber, rotor blades, stator blades, and turbine disc (13-15%), [–]

δ	– thickness, [m]
ε	– emissivity, [–]
η	– efficiency, [–]
μ	– dynamic viscosity, [kgm ⁻¹ s ⁻¹]
σ	– Stephan-Boltzmann constant (5.67·10 ⁻¹¹ kWm ⁻² K ⁻⁴)

Subscripts

AC	– air compressor
AP	– air preheater
a	– air
C	– convection
CC	– combustion chamber
c	– cooling air
f	– fuel
GT	– gas turbine
g	– combustion gases
gj	– gas flow ($j = 4, 5, 6$)
h	– hydraulic
K	– conduction
pz	– primary zone of the combustor
R	– radiation

References

- [1] Bejan, A., *Advanced Engineering Thermodynamics*, 2nd ed., John Wiley & Sons, New York, USA, 1997
- [2] Teixeira, V., *et al.*, Effects of Deposition Temperature and Thermal Cycling on Residual Stress State in Zirconia-Based Thermal Barrier Coating, *Surface and Coatings Technology*, 120-121 (1999), Nov., pp. 103-111.
- [3] DeMasi-Marcin, J. T., Gupta, D. K., Protective Coatings in the Gas Turbine Engine, *Surface and Coatings Technology*, 68-69 (1994), Dec., pp. 1-9
- [4] Johner, G., Schweitzer, K. K. J., Flame Rig Testing of Thermal Barrier Coatings and Correlation with Engine Results, *Journal of Vacuum Science & Technology, A: Vacuum, Surfaces, and Films*, 3 (1985), 6, pp. 2516-2524
- [5] Cernuschi, F., *et al.*, Thermal Diffusivity/Microstructure Relationship in Y-PSZ Thermal Barrier Coatings, *Journal of Thermal Spray Technology*, 8 (1999), 1, pp. 102-109
- [6] Risk, N. K., Mongia, H. C., Semianalytical Correlations for NO_x, CO and UHC Emissions, *Journal of Engineering for Gas Turbine and Power*, 115 (1993), 3, pp. 612-619
- [7] Clyne, T. W., Gill, S. C., Residual Stresses in Thermal Spray Coatings and Their Effect on Interfacial Adhesion: A Review of Recent Work, *Journal of Thermal Spray Technology*, 5 (1996), 4, pp. 401-418
- [8] Teixeira, V., *et al.*, Failure in PVD-Plasma Spraying Thermal Barrier Coatings During Thermal Cycling, *Proceedings* (Ed. C. Berndt), 8th National Thermal Spray Conference, Houston, Tex., USA, 1995, pp. 515-520
- [9] Chang, G., Phucharoen, W., Miller, R., Behavior of Thermal Barrier Coatings for Advanced Gas Turbine Blades, *Surface and Coatings Technology*, 30 (1987), 1, pp. 13-28
- [10] Evans, A. G., He, M. Y., Hutchinson, J. W., Mechanics-Based Scaling Laws for the Durability of Thermal Barrier Coatings, *Progress in Materials Science*, 46 (2001), 3-4, pp. 249-271
- [11] Evans, A. G., *et al.*, Mechanisms Controlling the Durability of Thermal Barrier Coatings, *Progress in Materials Science*, 46 (2001), 5, pp. 505-553
- [12] Thompson, J. A., Clyne, T. W., The Effect of Heat Treatment on the Stiffness of Zirconia Top Coats in Plasma-Sprayed TBCs, *Acta Materialia*, 49 (2001), 9, pp. 1565-1575

- [13] Vassen, R., et al., New Materials for Advanced Thermal Barrier Coatings, *Proceedings* (Eds. J. Lecomte-Beckers, F. Schuber, P. J. Ennis), 6th Liège Conference on Materials for Advanced Power Engineering, Liège, Belgium, 1998, pp. 1627-1635
- [14] Vaßen, R., Stöver, D., Functional Gradient Materials and Surface Layers Prepared by Fine Particles Technology, Kluwer Academic Publishers, Dordrecht, The Netherlands, 2001, pp. 199-216
- [15] Portinha, A., et al., Characterization of Thermal Barrier Coatings with a Gradient in Porosity, *Surface and Coatings Technology*, 195, (2005), 2-3, pp. 245-251
- [16] Portinha, A., et al., Stabilization of ZrO₂ PVD Coatings with Gd₂O₃, *Surface and Coatings Technology*, 188-189 (2004), Nov.-Dec., pp. 107-115
- [17] Raghavan, S., et al., Thermal Properties of Zirconia Co-Doped with Trivalent and Pentavalent Oxides, *Acta Materialia*, 49 (2001), 1, pp. 169-179
- [18] Nicholls, J. R., et al., Methods to Reduce the Thermal Conductivity of EB-PVD TBCs, *Surface and Coatings Technology*, 151-152 (2002), Mar., pp. 383-391
- [19] Stöver, D., Funke, C., Directions of Developments, of Thermal Barrier Coatings in Energy Applications, *Journal of Materials Processing Technology*, 92-93 (1999), pp.195-202
- [20] Siegel, R., Spuckler, C. M., Analysis of Thermal Radiation Effects on Temperatures in Turbine Engine Thermal Barrier Coatings, *Materials Science and Engineering: A*, 245 (1998), 2, pp. 150-159
- [21] Campagnoli, E., Ruscica, G., Factors Affecting the Application of Coatings on Superalloys, *High Temperatures – High Pressures*, 31 (1999), 3, pp. 321-329
- [22] Valero, A., et al., CGAM Problem: Definition and Conventional Solution, *Energy*, 19 (1994), 3, pp. 279-286
- [23] Yunus, A. Ç., Michael, A. B., Thermodynamics: An Engineering Approach, 3rd ed., McGraw-Hill, New York, USA, 1998
- [24] Cohen, H., Rogers, G. F. C., Saravanamuttoo, H. I. H., Gas Turbine Theory, 4th ed., Longman Group Ltd., UK, 1996
- [25] Kotas, T. J., The Exergy Method of Thermal Plant Analysis, Butterworths, Academic Press, London, 1985
- [26] Lazzaretto, A., Toffolo, A., Energy, Economy and Environment as Objectives in Multi-Criterion Optimization of Thermal Systems Design, *Energy*, 29 (2004), 8, pp. 1139-1157
- [27] Aydin, O., et al., Theoretical Analysis of Heat Transfer through an Idealized Gas Turbine Blade Model with Thermal Barrier Coating, *International Journal of Rotating Machinery*, 8 (2002), 2, pp. 81-86
- [28] Lefebvre, A. H., Gas Turbine Combustion, 2nd ed., CRC Press, Boca Ration, Fla., USA, 1998
- [29] Bejan, A., Kraus A. D., Heat Transfer Handbook, John Wiley & Sons Inc., Hoboken, N. J., USA, 2003

Authors' affiliations:

I. V. Ion (corresponding author)

"Dunarea de Jos" University of Galati,
Thermodynamics and Heat Engines Department
47, Domneasca Str., 800008 Galati, Romania
E-mail: ion.ion@ugal.ro

A. Portinha, V. Teixeira, J. Carneiro
University of Minho, Physics Department,
GRF-Functional Coatings Group,
Campus de Azurém, Guimarães, Portugal

J. Martins
University of Minho,
Mechanical Engineering Department
Campus de Azurém, Guimarães, Portugal

Paper submitted: February 22, 2008

Paper revised: September 12, 2008

Paper accepted: December 8, 2008